Dual-Band, Dual-Sense Textile Antenna with AMC Backing for Localization using GPS and WBAN/WLAN

IEEE Access
Multidisciplinary | Rapid Review | Open Access Journal

Date of publication xxxx 00, 0000, date of current version xxxx 00, 0000.

Digital Object Identifier 10.1109/ACCESS.2017.Doi Number

Dual-Band, Dual-Sense Textile Antenna with AMC Backing for Localization using GPS and WBAN/WLAN

RAHIL JOSHI[1,5], EZZATY FARIDAH NOR MOHD HUSSIN[2], PING JACK SOH[2], MOHD FAIZAL JAMLOS[3], HERWANSYAH LAGO[4], AZREMI ABDULLAH AL-HADI[2] and SYMON K. PODILCHAK[1,5]

[1]Institute of Sensors, Signals and Systems (ISSS), Heriot Watt University, Edinburgh EH14 4AS, United Kingdom.
[2]Advanced Communication Engineering Centre (ACE) Centre of Excellence (CoE), School of Computer & Communication Engineering, Universiti Malaysia Perlis, Malaysia.
[3]Faculty of Mechanical Engineering, Universiti Malaysia Pahang, 26600 Pekan, Pahang.
[4]Faculty of Engineering, Universiti Malaysia Sabah, 88400 Kota Kinabalu, Sabah, Malaysia.
[5]Department of Engineering, University of Edinburgh, EH9 3FB, United Kingdom.

Corresponding author: Ping Jack Soh (pjsoh@unimap.edu.my) and Symon K. Podilchak (s.podilchak@ed.ac.uk)

This project was supported in part by the Malaysia Ministry of Education under the Fundamental Research Grant Scheme (FRGS) (grant no: FRGS/1/2015/ICT05/UNIMAP/02/2), and the MyBrain15 Scholarship. This work was also supported by the European Union's Horizon2020 Research and Innovation Program through Marie Sklodowska-Curie under Grant 709372 and in part by the EU H2020 ITN REVOLVE project under Grant 722840. The authors would like to indicate that the work is only the authors' views, and that the Horizon 2020 Agency is not responsible for any information contained in the letter.

ABSTRACT A wearable textile antenna with dual-band and dual-sense characteristics is presented in this work. It operates at the 2.45 GHz band for WBAN and WLAN applications, and at the 1.575 GHz band for Global Positioning System (GPS) applications. An antenna backing based on an artificial magnetic conductor (AMC) plane operating at 2.45 GHz band is introduced to reduce the backward radiation and to improve antenna gain. It consists of a 3×3 array of square patch unit cells, where each unit cell is integrated with four square slits and a square ring. A square-shaped patch is then located on top of the substrate as its radiator. To enable dual-band operation, two corners of this radiator are truncated, with each of the four corners incorporated with a rectangular slit to enable its circular polarization characteristic in the GPS band. Simulation and experimental results are in good agreement and indicate proper antenna operation with linear polarization in the 2.45 GHz band and circular polarization in the 1.575 GHz band, with realized gain of 1.94 dBi and 1.98 dBic, respectively.

INDEX TERMS Dual-band dual-sense antenna, wearable antenna, AMC plane.

I. INTRODUCTION

Research on wearable antennas has been intensive in recent years due to its huge potential generated for integrating wireless capability into clothing. Textiles has been the preferred material due to their comfort, light weight, high flexibility, and ease of integration with clothing [1]. Such implementation is especially useful in location tracking especially in search and rescue, and also, long-term patient monitoring [2]. Due to these advantages, researchers have envisioned the use of the two widely available methods suitable in both indoor and outdoor for wireless localization: using WLAN for the former, and using the Global Positioning System (GPS) for the latter, using a single antenna. This technology merging using a single wearable device based on textile technology is highly cost-effective, besides improving the comfort for the user [1]. However, the use of such radiators in the vicinity of users typically results in coupling to the human tissues and electromagnetic absorption into parts of the body, especially in the lower microwave frequencies with longer signal wavelengths. Concerns on health may arise if the level of this absorption does not meet its regulatory requirements, defined in terms of Specific Absorption Rate (SAR) [3]. One of the effective methods in reducing the SAR level is by shielding the radiator of the antenna from the body using conventional metallic planes or metasurfaces such as AMC planes.

The concept of integrating dual- and multi-frequency antennas is popular in multi-functional wireless products, as it effectively reduces the required number of components and effectively of the hardware. For instance, the dual-frequency antennas in [4-5] are capable of providing operation in different operating bands with unique radiation features to suit their applications. Meanwhile, the use of circularly-polarized (CP) antennas is advantageous in wireless communications as they allow signal reception irrespective of the orientation of the receiving antenna with respect to the transmitting antenna. This consequently results in the suppression of multipath interference. On the contrary, there needs to be a proper polarization alignment for linearly-polarized antennas when in operation to ensure efficient signal transmission and reception. Meanwhile, it is much less complex to design dual- or multiband linearly polarized antennas in comparison to CP antennas operating in multiple bands, making the former the preferred choice for localization in an indoor environment.

Two commonly known methods by which circular polarization can be achieved are: (1) truncating corners of the patch and (2) by introducing a slit aligned with the diagonal axis of the patch. In [6], an analysis on three different types of CP patch antennas were reported using a Green's function approach and the desegmentation method. It was found that circular polarization for conventional patch antennas has largest axial ratio bandwidth and can be achieved using a square patch with a diagonal slit, whereas the corner-truncated patch can be used to achieve the best axial ratio levels. In [7], four asymmetric slits were introduced in the diagonal directions to achieve circular polarization. In addition to that work, a patch antenna was designed with truncated corners and four slits with good matching and axial ratio at the operational frequency [8]. Most importantly, the adoption of such a technique effectively miniaturized the size of the antenna by about 36 %.

On the other hand, the implementation of metasurfaces within antenna designs has increased rapidly in recent years, mainly due to their capability in widening the axial ratio bandwidth and enhancing realized gain. A review on different antenna designs integrated with AMC surfaces was reported in [9]. Besides that, a circular cross slit AMC design was also proposed to improve radiation and enhance bandwidth for UWB antennas. Wide bandwidths are also significant for 5G applications. For example, the bandwidth of a CP patch antenna with a metasurface was reported to be 34.7% in [10] (that is approximately 26 % better than the antennas which are not integrated with metasurfaces). Similarly, a partially reflected surface (PRS) was used to broaden the bandwidth of a CP Fabry-Perot antenna in [11].

Considering the aforementioned factors, this work aims to design, for the first time and to the best knowledge of authors, a dual-band and dual-sense (linear and circular polarization) textile antenna backed using an artificial magnetic conductor (AMC) plane. This configuration provides further antenna miniaturization and suppression of backward radiation, besides improving gain and bandwidth [12-15], which are extremely attractive features for wearable devices. A preliminary investigation in free space and under bent conditions was presented in [16]. Ultimately, the proposed antenna is capable of a dual-band and dual-sense operation: 1) for indoor wireless localization using WLAN/WBAN standards, operating with linear polarization; as well as; 2) for outdoor location tracking using the GPS standard, operating with circular polarization. Both operations require radiation with their respective linear and circular polarizations, with the proposed body worn antenna radiating outwards from the body.

The next section will first explain the design procedure for the patch and the AMC unit cell, followed by the design of the AMC plane and the top radiator, prior to their integration (see Figs. 1 to 3). Results from simulations and measurements are then presented in Section 3. Finally the concluding remarks are summarized in Section 4.

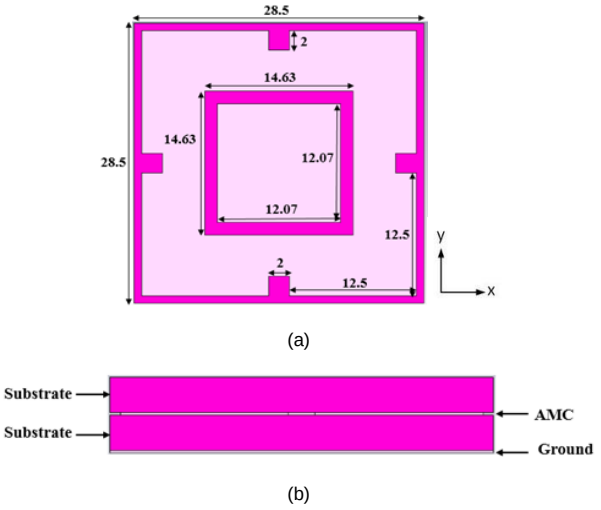

FIGURE 1. AMC unit cell (a) Dimensions of the AMC unit cell (in mm) and (b) AMC unit cell cross section with a substrate thickness of 2.64 mm per layer and conductor (AMC and ground) thickness of 0.17 mm per layer.

II. AMC SURFACE and ANTENNA DESIGN

The unit cell of the AMC plane is designed based on a square patch, as illustrated in Figure. 1(a). This patch is then integrated with a square ring centered on this patch. This is followed by the addition of four square slits centered at each of its sides. The AMC unit cell is built using four layers of materials, as illustrated in Figure. 1(b). The bottom-most layer is the ground plane. A layer of felt substrate is placed on top of it, followed by the AMC unit cell. Another subsequent felt substrate layer is placed on top of this AMC unit cell layer, prior to the placement of the radiator on top of this felt substrate layer. The AMC cells and ground plane are built using a conductive textile, ShieldIt Super, which is 0.17 mm thick and is highly conductive (with 1.18×10^5 S/m). The substrate, on the other hand, is made using Kevlar, which has a permittivity (ε_r), of 1.66, a loss tangent (tan-δ)

of 0.0704 measured at 2.45 GHz, and is 2.64 mm in thickness.

The periodic unit cell boundary condition available within CST Microwave Studio was used to perform the simulations and optimization aimed at obtaining the zero-degree reflection phase at 2.45 GHz. This structure is excited by a plane wave source placed at 10 mm distance from the top of the AMC cell. Its final reflection phase plotted in Fig. 2 validated its operation centered at 2.45 GHz with a bandwidth of 449 MHz. To form the AMC plane, this unit cell was then arranged into a 3×3 array.

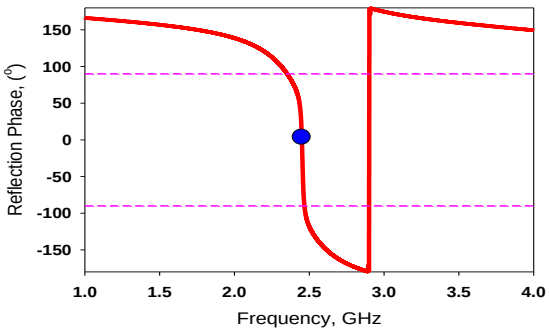

FIGURE 2. **Reflection phase of the AMC unit cell.**

It should be mentioned that the dimensions of the rectangular AMC unit cell can be calculated using the equations mentioned in [17]. The operating frequency can also be changed by tuning the relative dielectric constant of the substrate [18]. When bending the AMC unit cell by approximately 45° for the intended wearable applications, the reflection phase changes very slightly and still maintains its reflection phase from +90° to -90° at 2.45 GHz.

Next, the radiator of the antenna was designed. This radiator is intended for dual band operation in the 1.575 GHz and 2.45 GHz bands, as illustrated in Figure. 3. To enable a single-fed circularly polarized antenna structure, the square patch radiator is combined with a pair of truncated corners opposite to each other. The lengths of the truncated corners are optimized to be the same at 12 mm. Next, a rectangular slit is integrated onto each side of four corners of the patch to enable dual-band operation.

To further describe the design procedure for the proposed dual-band and dual-sense antenna, it starts from a simple linearly polarized square patch. Typically the antenna is fed from the bottom by a probe and the inner pin of the connector is extended to the patch. Three common ways to achieve circular polarization are: (1) by using a single, dual or more feeds [19], (2) trimming the opposite corners of the patch, and (3) introducing thin slits [20]. In the proposed design, a truncated corner technique was used to achieve circular polarization and four slits were inserted at each corner of the patch to enhance the bandwidth. The resulting surface current distribution at each design stage is illustrated in Fig. 4(a-d). The surface current distribution in the lower band for different phase (0˚, 90˚, 180˚ and 270˚) shows the changes in

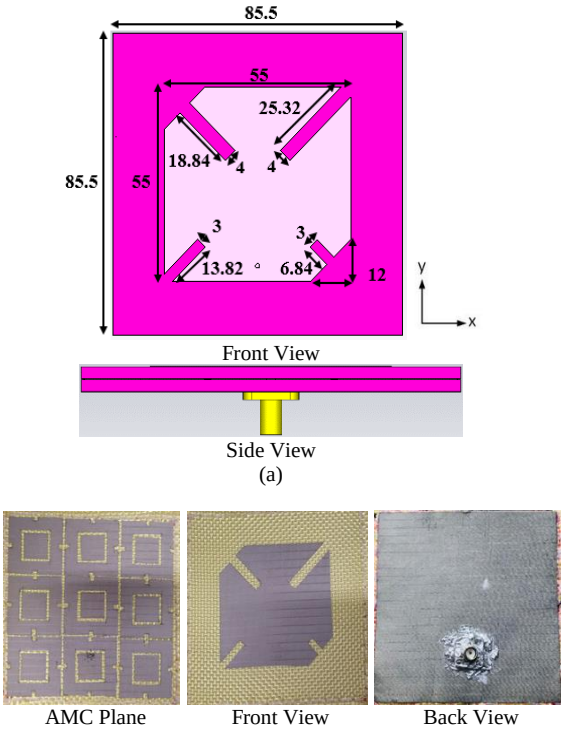

FIGURE 3. **Antenna design (a) topology of the dual-polarized planar textile antenna (al dimensions in mm) and (b) fabricated prototype.**

the current direction illustrating the CP characteristics of the proposed antenna.

It was initially observed that the position of the probe resulted in a dual-band polarization of the proposed antenna. But after further optimization, it was noticed that the slits were contributing towards resonance at the upper band frequency. This provided insight that the upper corners of the patch enabled resonance at 1.575 GHz, whereas the lower corners allowed operation at 2.45 GHz. The antenna can also be tuned to a single frequency operation by adjusting the two truncated corners in the structure. For example, by changing the size of top truncated corner length, one can tune the resonance in the lower frequency band (currently centered at 1.575 GHz). Likewise, tuning the 2.45 GHz frequency band can be performed by adjusting the slits in the lower corners of the antenna. Finally, an AMC plane was integrated beneath the optimized radiator, as illustrated in Figure. 3.

The overall dimension of the antenna with the AMC layer is 85.50 × 85.50 × 5.62 mm^3. The electrical length of the proposed antenna is $0.4\lambda_o \times 0.4\lambda_o \times 0.02\lambda_o$ at 1.575 GHz and $0.68\lambda_o \times 0.68\lambda_o \times 0.04\lambda_o$ at 2.45 GHz. It should also be mentioned that antenna structures of similar function have also been presented previously in the literature [15] but were slightly larger (110 × 110 × 10.2 mm^3), with capacitive slot-feeding, and employed a hybrid coupler chip to achieve CP operation at 1.575 GHz, and which, can increase design complexity. Our proposed antenna, instead, is a simple dual-band and dual-polarized patch antenna that is probe fed and is

TABLE I
AMC ARRAY SIZE VARIATION AND THICKNESS BETWEEN THE PATCH AND THE AMC PLANE (SIMULATIONS) WHEN PLACED ON THE BODY

Frequency Band	AMC Plane Size	Overall Antenna Structure Dimension (mm^2)	Thickness between AMC plane and patch (mm)	SAR (W/kg)	Radiation Efficiency (%)
Lower Band Frequency	2×2	61.5 × 61.5	1.62	0.59	35.9
			2.62	0.48	59.0
			3.62	0.62	63.5
	3×3 (Proposed)	**85.5 × 85.5**	1.62	0.38	63.3
			2.62 (Proposed)	**0.78**	**73.6**
			3.62	0.90	79.2
	4×4	115.5 × 115.5	1.62	0.25	60.6
			2.62	0.32	69.6
			3.62	0.54	75.5
Upper Band Frequency	2×2	61.5 × 61.5	1.62	0.62	59.1
			2.62	0.75	75.1
			3.62	0.98	77.5
	3×3 (Proposed)	**85.5 × 85.5**	1.62	0.52	76.5
			2.62 (Proposed)	**0.71**	**83.0**
			3.62	0.49	86.1
	4×4	115.5 × 115.5	1.62	0.12	77.9
			2.62	0.28	78.7
			3.62	0.42	84.7

*Radiation Efficiency = Peak Gain / Directivity, as defined in [22].

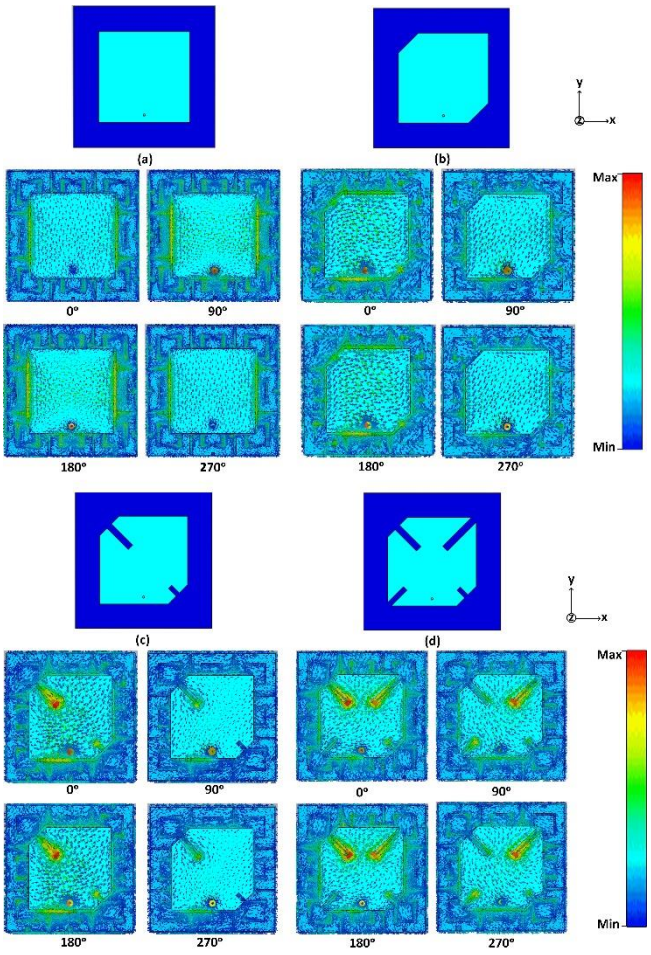

FIGURE 4. Step-by-step illustration of the proposed antenna design procedure. (a) Linear polarized patch antenna was designed at the lower band frequency. (b) Circular polarized patch antenna operational at the lower band frequency. (c) Patch antenna with diagonal slits operational at the upper band frequency. The integration of slits at the truncated corner introduced an upper band frequency resonance. (d) The proposed circular polarized patch antenna with four slits operational at 1.575 GHz and 2.45 GHz. The four slits at each corner of the patch helps to achieve dual band performance with better matching in the proposed antenna. Upper and lower corners of the patch can be tuned to single frequency operation. The surface current distribution in A/m at 1.575 GHz are shown for different phase values (at 0°, 90°, 180° and 270°) in each design to illustrate circularly polarized radiation.

realized by patterning of the various metallic layers (see Figs. 1 and 3).

An analysis was conducted to check the performance of the proposed antenna by changing the size of AMC array and thickness of the substrate between the patch and AMC plane (see Table I) considering off body radiation from a human phantom. Note that the size of AMC array changes the overall size of the antenna structure by at least ±35%. For example, a 2×2 AMC array is dimensioned at 61.5×61.5 mm^2 whereas the dimension of a 4×4 AMC array is 115.5×115.5 mm^2. The thickness of the proposed antenna was changed by ±1 mm by substrate thickness between the AMC plane and the patch, which is currently at 2.62 mm for the 3×3 array. Table 1 summarizes the performance of the proposed antenna with varying AMC array sizes and the substrate thickness in terms of radiation efficiency and SAR. It is observed that the radiation efficiency improves as the thickness of the antenna is increased in both frequency bands. It is valid that the thickness of the substrate increases the radiation efficiency but also the surface wave increases which is undesirable [21]. On the other hand, the SAR values are reduced when the antenna is integrated with a 4×4 AMC array, at the expense of a significant increase in the overall antenna size. This can be less practical due to the intended use of the proposed antenna on certain parts of the body such as the arms and shoulders, especially when bent. Moreover, the improvements in terms of radiation efficiency (of less than 10%) is not of major significance considering the 35 % increase in size when using 4×4 array instead of the 3×3

array, and their SAR levels are both well below the allowable regulatory level of 2.0 W/kg.

III. RESULTS AND DISCUSSION

A. PERFORMANCE IN FREE SPACE (PLANAR)

The proposed antenna performance is first studied in free space in terms of its reflection coefficient, bandwidth, and radiation patterns. However, the wearable antenna operation in a planar, free space condition is not the actual intended application, and thus will be studied briefly to obtain an approximate idea of its performance in ideal conditions. The results presented in Fig. 5(a) indicated that the proposed antenna operated with a simulated 10 dB impedance bandwidth of 120 MHz at 1.575 GHz. This translates into an equivalent fractional bandwidth of 7.6 %. Meanwhile at 2.45 GHz, results indicated a simulated bandwidth of 136 MHz, which is about 5.5 % of equivalent fractional bandwidth.

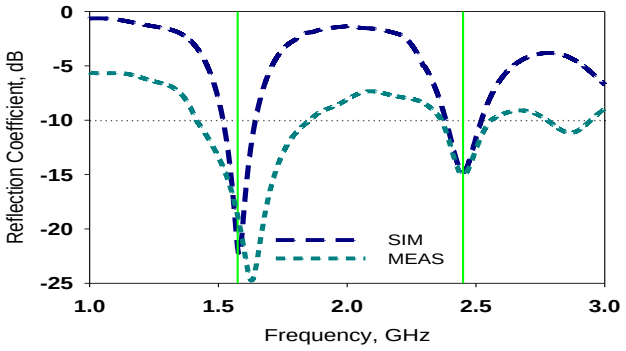

(a)

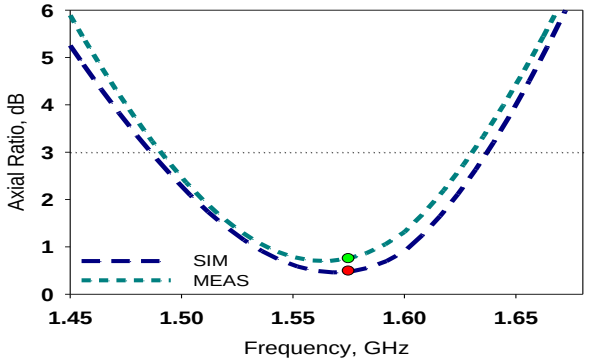

(b)

FIGURE 5. Simulated and measured results of the antenna performance: (a) reflection coefficient; and (b) axial ratio.

During measurements, the proposed structure is validated to operate with 185 MHz of bandwidth at 2.45 GHz and 440 MHz of bandwidth at 1.575 GHz. Their equivalent fractional bandwidth is 27 % and 7.5 % at 2.45 GHz and 1.575 GHz, respectively. In free space, dual-polarization is already evident from both the simulations and measurements by observing its axial ratio in the 1.575 GHz band. Results in Figure 5(b) showed that the proposed antenna features a 10.3 % of circular polarization axial ratio bandwidth when simulated, and 9 % when measured in this band. Besides that, simulation and measurement results also indicated a linear polarization behavior in the 2.45 GHz band. Moreover, the movement of surface current in a circular direction in the proposed antenna (at 1.575 GHz) can be observed in Figure 4(d). Also, the operation of the AMC plane at 2.45 GHz resulted in a realized gain of about 2 dBic at 1.575 GHz and 1.9 dBi at 2.45 GHz. Figure 6(a) and (b) reports the measured and simulated realized gain across the lower and upper frequency ranges and results are in good agreement with the simulations. The radiation efficiency of the proposed antenna with the AMC plane at 1.575 GHz and 2.45 GHz are 73.6% and 83%, respectively. The radiation efficiency of the proposed design without the AMC plane at 1.575 GHz and 2.45 GHz are 48% and 45%, respectively. Adding an AMC plane enhances the overall performance of the antenna.

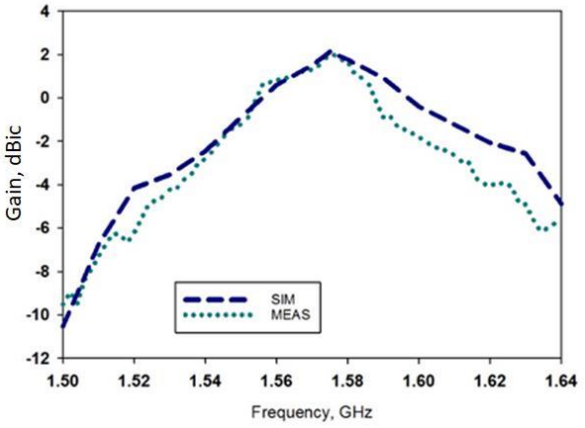

(a)

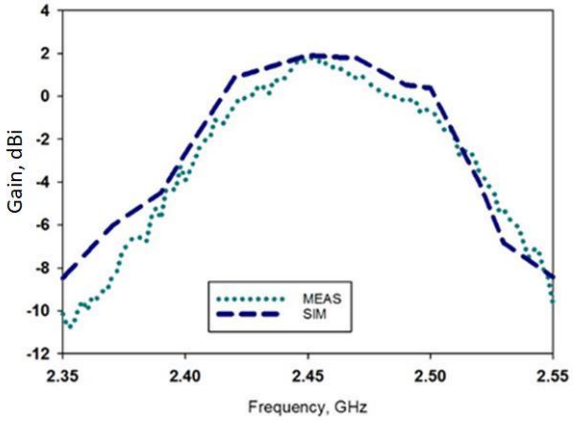

(b)

FIGURE 6. Simulated and measured realized gain across two frequency ranges when the antenna is in free space (a) lower band frequency (1.575 GHz) and (b) upper band frequency (2.45 GHz).

B. PERFORMANCE IN FREE SPACE (BENT)

It is foreseen that the antenna will suffer physical deformation during operation due to the flexible textile materials used to build it. Thus, this section is dedicated to study the effects of the antenna independently when bent in

free space using simulations and measurements. This followed by the investigation of its performance in the following section when bent and placed over a detailed human voxel model.

The first investigation is performed by conformally bending the proposed antenna around a cylinder with a radius of r = 60 mm at the x- and y-axes, as illustrated in Figure 7. This is done to simulate its placement when worn on the upper arm. The simulated and measured reflection coefficients of the proposed antenna when evaluated under bending in free space are presented in Figure 8. Simulations indicated that the antenna bending at the x-axis slightly increased its bandwidth from 120 MHz to 160 MHz when compared to its planar form in the 1.575 GHz band. Meanwhile, bandwidth in the 2.45 GHz band is also increased from 136 MHz to 190 MHz when compared to its planar representation. The axial ratio of the antenna is found to be 2.2 dB when the antenna is bent to 45°. The axial ratio in this bent condition is approximately 1.2 dB higher than in its planar form (see Fig. 5(b)). Nonetheless, the AR is still below 3 dB and the antenna maintains CP operation at 1.575 GHz.

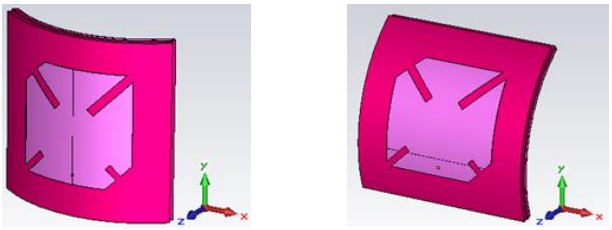

(a) (b)

FIGURE 7. The antenna when bent at the (a) *y*-axis and (b) *x*-axis

On the contrary, the antenna bent at the y-axis increased the bandwidth in the 1.575 GHz band to 140 MHz in simulations, and to 164 MHz in the 2.45 GHz band. Meanwhile, when the antenna structure is bent at the x-axis, its bandwidth is decreased to 300 MHz in the 1.575 GHz band. In comparison, measurements in planar form resulted in a bandwidth of 440 MHz. In the WLAN/WBAN band, the bandwidth is reduced from 185 MHz (in planar form) to 110 MHz when the antenna is bent at the x-axis. On the other hand, bending of the proposed antenna at the y-axis indicated a bandwidth reduction in both 1.575 GHz band (to 255 MHz) and 2.45 GHz band (to 85 MHz).

Generally, the antenna performance considering all bent configurations are almost identical to its performance in planar form, with slight fluctuations in reflection coefficient and bandwidth compared (see Fig. 8). This is in agreement with the findings from [23], where the smaller bending radius resulted in a shorter resonant length in comparison with its planar form. When the antenna is bent at the y-axis, a relatively larger bandwidth reduction is exhibited in comparison to the x-axis bending. This observation is aligned with the findings in [23], where the existence of the AMC plane alleviated the effects of the bending.

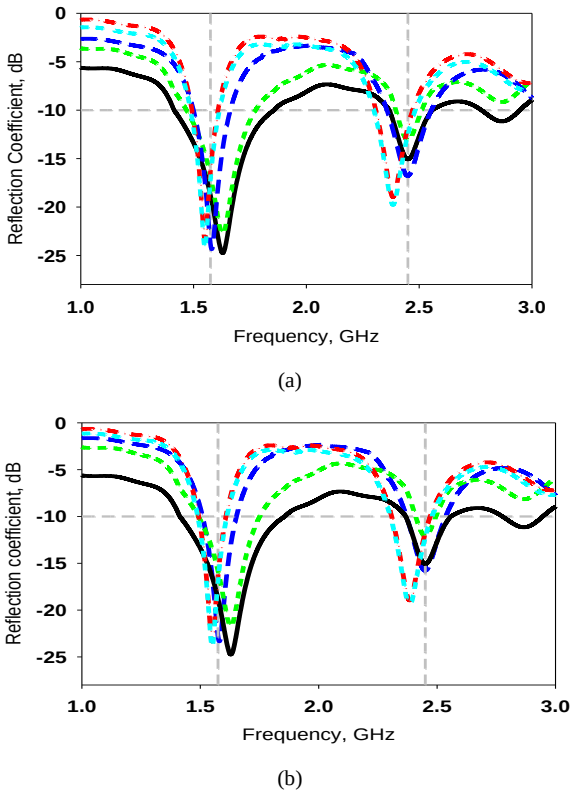

FIGURE 8. Antenna reflection coefficients when bent at the (a) *x*-axis and (b) *y*-axis. Legend: measured planar antenna (solid black line); bent with r = 60 mm (simulated) (long dashed blue line); bent with r = 60 mm (measured) (short dashed green line); bent on shoulder (dashed-dot red line); bent on upper arm (short-short cyan line).

The results observed after bending is similar to the findings in [23], where the EBG was used as a substrate and due to the presence of this EBG plane, the bending has a minimal effect on the antenna performance. Also, an EBG and AMC do not offer the same physical response in support of the antenna operation for the intended textile application, but yet can also be made using grounded dielectrics, and textile materials as in this work, and for multiband operation as in [24].

To analyze further the performance of the antenna in its bent form (approx. 30°), the surface current distribution was studied. Figure 9 illustrates the surface current distribution of the antenna in planar and its bent form at the two resonant frequencies. The amplitude of the surface current in planar and bent form at 1.575 GHz are 88.4 A/m and 88.5 A/m, respectively. Likewise, at 2.45 GHz they are 58.7 A/m and 58.3 A/m, respectively.

Regardless of these minor changes in the surface current distributions and observed maximums (see Fig. 9), satisfactory performance of the antenna is observed under both bent conditions and when operating in free-space. To quantify the impact of the AMC plane in decreasing backwards radiation for these scenarios, the front-to-back ratios (FBRs) are assessed both in terms of simulations and measurements at 1.575 GHz and 2.45 GHz (see Table I). The simulated FBR of the antenna in planar form is initially 19.6 dB (at 1.575 GHz)

and 17.4 dB (at 2.45 GHz). The antenna FBR is then reduced to 15.9 dB at 1.575 GHz and to 10 dB at 2.45 GHz when bent at the *x*-axis. Meanwhile, the antenna's simulated FBR also decreased to 11.6 dB at 1.575 GHz and 10.9 dB at 2.45 GHz when bent at the *y*-axis.

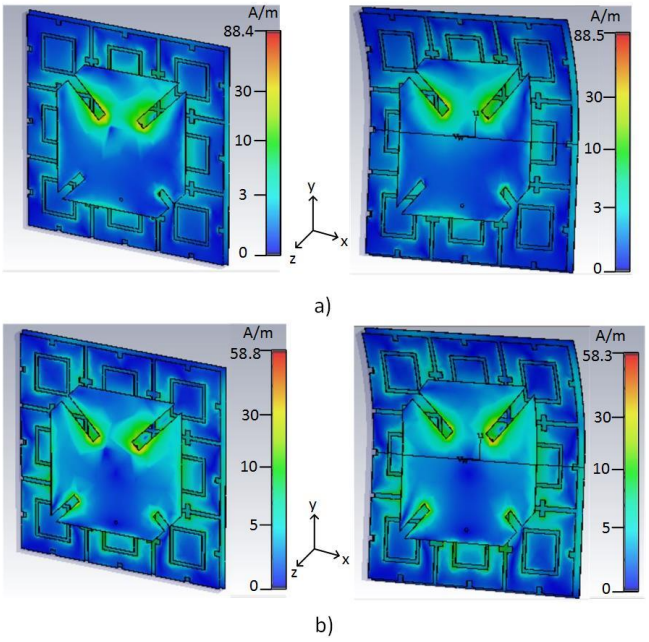

FIGURE 9. **Amplitude of surface current distribution for planar and bent form at (a) 1.575 GHz and (b) 2.45 GHz.**

TABLE II
SIMULATIONS OF THE ANTENNA AND THE FRONT-BACK-RATIO WITH AND WITHOUT THE AMC PLANE

Frequency (GHz)	Condition	FBR (dB)
1.575	Planar with AMC	19.6
	Bent with AMC	10.2
	Planar without AMC	13.4
	Bent without AMC	9.1
2.45	Planar with AMC	17.4
	Bent with AMC	10.0
	Planar without AMC	11.3
	Bent without AMC	11.0

Measurements when the antenna is bent at the *x*-axis produced FBR levels of 12.89 dB at 1.575 GHz, and 15.51 dB at 2.45 GHz. In contrast, the measured FBR of the planar antenna in free space is 9.64 dB. Meanwhile, the measured FBR when bent at the *y*-axis are less affected, with FBR degradations to 14.83 dB (at 1.575 GHz) and 9.48 dB (at 2.45 GHz). On the other hand, the simulated and measured radiation patterns of the antenna when bent at the two directions are illustrated in Figure 10. As intended, the antenna radiated towards the broadside with low backlobes, minimizing radiation towards the human user. The simulated FBR of the antenna in planar form at both frequencies are summarized in Table II when antenna is with and without the AMC plane. It can be observed

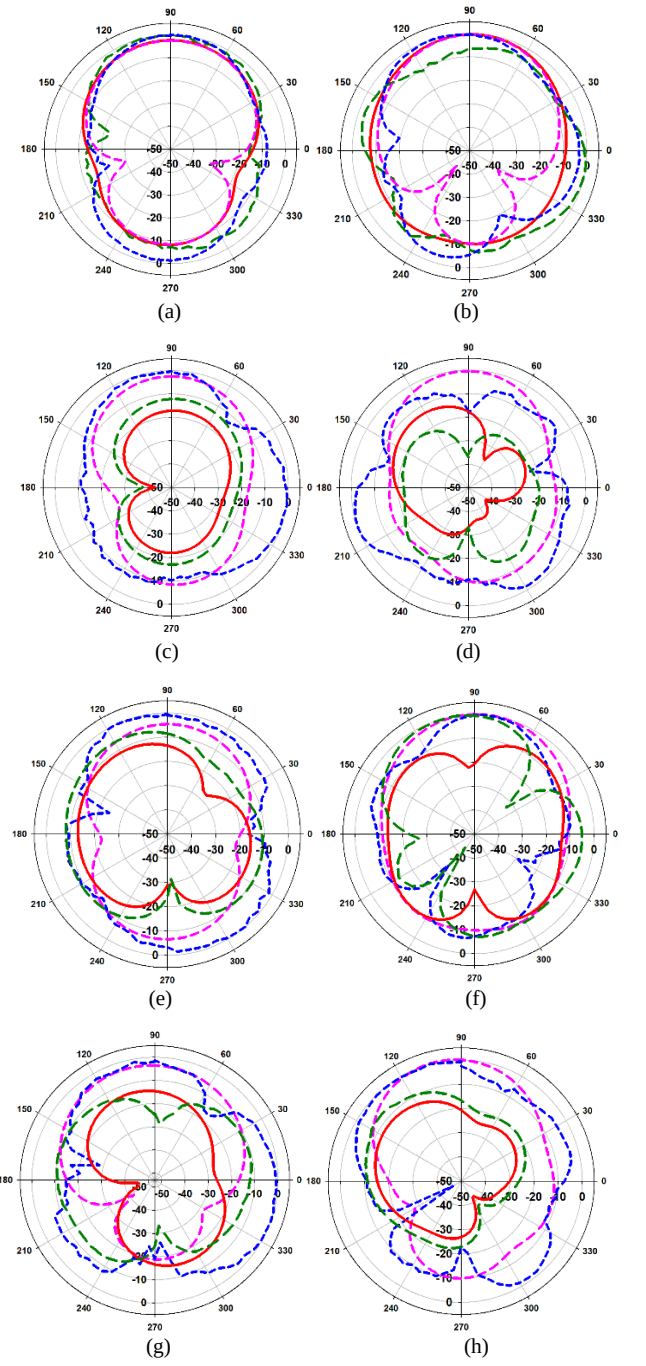

FIGURE 10. **Simulated and measured radiation patterns of the proposed antenna when bent at the (a) *x*-axis (*xz*-plane) at 1.575 GHz, (b) x-axis (*xz*-plane at 2.45 GHz), (c) *x*-axis (*yz*-plane) at 1.575 GHz, (d) *x*-axis (*yz*-plane) at 2.45 GHz, (e) the *y*-axis (*xz*-plane) at 1.575 GHz, (f) the *y*-axis (*xz*-plane) at 2.45 GHz, (g) *y*-axis (*yz*-plane) at 1.575 GHz and (h) *y*-axis (*yz*-plane) at 2.45 GHz. Legend: simulated co-polarization (medium dashed pink line); simulated cross-polarization (solid red line); measured co-polarization (short dashed blue line); measured cross-polarization (long dashed dark green line).**

that the FBR is lower for the antenna structure without the AMC plane as compared to the proposed antenna structure in planar and bent form. These results suggest that the AMC plane does indeed reduce backward radiation.

C. PERFORMANCE ON-BODY (BENT)

Next, the on-body performance of the bent antenna in proximity of the body is further validated using a voxel model. Simulations are performed using the bent antenna placed at a 10 mm distance over the truncated shoulder and upper arm of a Hugo voxel model (using $1 \times 1 \times 1$ mm^3 mesh resolution) to reduce computational resources. The 10 mm distance is determined based on an average clothes-to-body spacing which varies with time and user's movements, assuming that the clothes worn is with average tightness. For simulations and measurements, the antenna was placed at the upper arm (UH) and shoulder (SH) of the human body. In these studies, the shoulder has a radial geometry and was chosen to achieve bending of the antenna along the x-axis acting as if the antenna is placed on a circular object. Also, the bending in the y-axis was achieved by placing the antenna at the upper arm of the human body.

Simulations are performed using the bent antenna placed at a 10 mm distance over the truncated shoulder and upper arm of a Hugo voxel model (using $1 \times 1 \times 1$ mm^3 mesh resolution) to reduce computational resources. The 10 mm distance is determined based on an average clothes-to-body spacing which varies with time and user's movements, assuming that the clothes worn is with average tightness [25].

Evaluation when the antenna is bent at the *x*-axis over the upper arm altered the bandwidth to 120 MHz in the 1.575 GHz band and 172 MHz in the 2.45 GHz band. Conversely, bending at the *y*-axis produced a bandwidth of 120 MHz in the 1.575 GHz band and 172 MHz in the 2.45 GHz band. When simulated over the shoulder and bent at the *x*-axis, the bandwidth in the 1.575 GHz band decreased to 112 MHz and to 156 MHz in the 2.45 GHz band. On the contrary, *y*-axis bending of the antenna did not affect the bandwidths, as a similar 112 MHz of bandwidth is shown in the 1.575 GHz band, and 156 MHz is produced in the 2.45 GHz band. It is also concluded that the antenna can be operated when bent on body at the *y*-axis, as this increased bandwidths in both the 1.575 GHz and 2.45 GHz bands. These results are illustrated in Figure 8.

TABLE III
SUMMARY OF BENT ON-BODY EVALUATIONS

Freq. (GHz)	Cond. (Sim)	SAR (W/kg)		Bandwidth (MHz)		FBR (dB)	
		UA	SH	UA	SH	UA	SH
1.575	*x*-axis	0.111	0.098	120	112	16.0	11.6
	y-axis	0.086	0.045	120	112	15.3	15.4
2.45	*x*-axis	0.111	0.075	172	156	10.3	23.3
	y-axis	0.088	0.057	172	156	11.2	26.1

On the other hand, simulations for FBR indicated levels of 16.03 dB when the antenna is bent at the *x*-axis on the upper arm at 1.575 GHz, whereas this is reduced to 10.3 dB at 2.45 GHz. Evaluation of the antenna bent at the *y*-axis when placed on the upper arm showed FBR values of 15.3 dB (at 1.575 GHz) and 11.2 dB (at 2.45 GHz). When bent on the shoulder at the *x*-axis, the simulated FBR for the antenna is 11.6 dB and 23.3 dB at 1.575 GHz and 2.45 GHz, respectively. When bent over the shoulder at the *y*-axis, an increased FBR at both frequencies can be observed, which is 15.4 dB (at 1.575 GHz) and 26.1 dB (at 2.45 GHz).

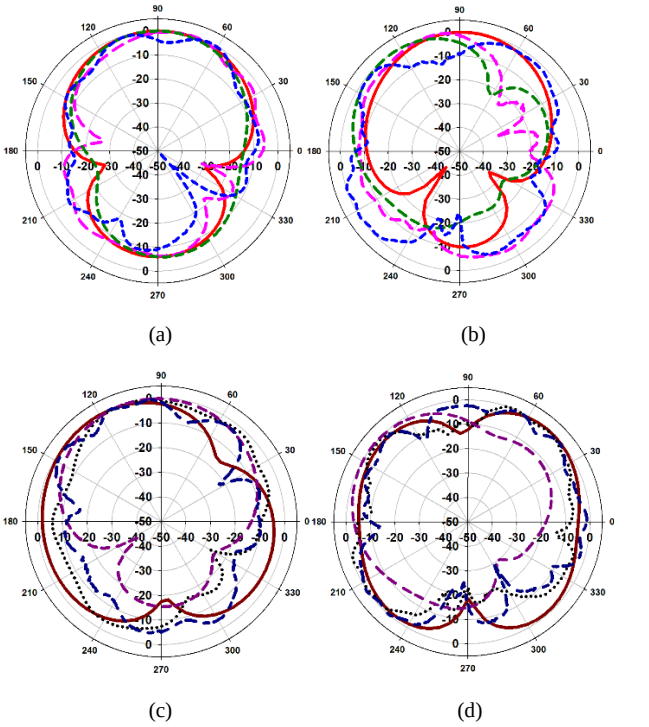

FIGURE 11. Simulated and measured radiation patterns at the *yz*-plane when the antenna is placed on the upper arm and shoulder at (a) 1.575 GHz bent at the *x*-axis, (b) 2.45 GHz bent at the *x*-axis, (c) 1.575 GHz bent at the *y*-axis and (d) 2.45 GHz bent at the *y*-axis. Legend: Simulation and measurement at the upper arm when bent on *x*-axis (solid red line and long dashed pink, respectively) and on the shoulder when bent at the *x*-axis (medium dash dark green and short dash blue, respectively); Simulation and measurement at the upper arm when bent on *y*-axis (solid dark red line and dotted black, respectively) and on the shoulder when bent at the *y*-axis (medium-medium dark pink and long-short dark blue, respectively).

In general, the antenna operated on the body when bent at both the *x*- and *y*-axes and resulted in an increment of FBR compared to the antenna in free space, as illustrated in Figure 10. There are some minor discrepancies in Figs. 10(b) and (d) between the simulated and measured results. This is due to the probe and SMA feed used for the antenna, making it rather difficult for uniform bending on the mannequin. Regardless, the antenna still maintains its performance and front back ratio is in close agreement with the simulations.

Notice also that while the antenna impedance bandwidths when bent at both axes and evaluated near both locations (upper arm and shoulder) are similar, significant improvements in FBR are observed when the antenna is operating at 2.45 GHz. This is expected from the shielding provided by the AMC plane backing which operated most efficiently in this particular band.

The final assessment for the proposed antenna is performed in terms of safety. It is based on the standards set by the International Commission on Non-Ionizing Radiation

TABLE IV
COMPARISON OF PROPOSED ANTENNA WITH PREVIOUS MULTIBAND ANTENNAS WITH DUAL SENSE (LINEAR AND CIRCULAR) POLARIZATIONS

Ref.	Main Topology	Freq. (GHz)	Polarization	Fractional Bandwidth (%)	Peak Gain (dBi/dBic)	Axial Ratio (%)	FBR (dB)	Flexible
[13]	Planar Monopole	1.88	Circular	7.5	3.95	2.7	6.5	No
		2.5	Circular	12.6	5.29	2.0	7.0	
[26]	Patch antenna (sim only)	3.6	Circular	7.5	8.5	0.7	-	No
		5.2	Linear	9.5	8.6	-	-	
[27]	Patch antenna	1.76	Linear	1.4	2.11	-	-	No
		2.55	Circular	1.3	-3.9	1.25	-	
		3.85	Linear	2.6	2.5	-	-	
[28]	Patch antenna	4.0	Linear	-	5.0	-	-	No
		5.0	Circular	9.4	5.0	4.0	-	
[29]	Patch antenna	1.38	Linear	2.0	2.0	-	-	No
		1.57	Circular	1.0	7.0	1.3	-	
[30]	Patch antenna	1.575	Circular	1.8	5.1	0.7	21.9	Semi-flex
		2.45	Linear	1.6	5.0	-	24.5	
Proposed antenna	Patch antenna	1.575	Circular	7.6	1.98	10.3	16.7	Yes
		2.45	Linear	5.5	1.94	-	12.0	

Protection (ICNIRP) [3], and is regulated at a maximum of 2 W/kg averaged over 10 g of tissue. Assessments were performed using CST with a 0.5 W_{rms} input power fed into the antennas located at the same distance over the same voxel models of the upper arm (UA) and shoulder (SH). When bent at the *x*-axis and placed on the upper arm, the antenna configuration produced SAR values of 0.111 W/kg at 1.575 GHz and 0.111 W/kg at 2.45 GHz. Meanwhile, when bent at the *y*-axis on placed in proximity of the upper arm, this setup resulted in 0.086 W/kg and 0.0877 W/kg of SAR at 1.575 GHz and 2.45 GHz, respectively.

When bent at the *x*-axis and placed on the shoulder, the resulting SAR value of the antenna is 0.0983 W/kg at 1.575 GHz and 0.0747 W/kg at 2.45 GHz. The antenna bent at the *y*-axis and located near the shoulder resulted in 0.0449 W/kg and 0.0573 W/kg of SAR at 1.575 GHz and 2.45 GHz, respectively. These values indicate safe operation in the vicinity of the body as they are well below the regulated SAR limits which were simulated to be 0.134 W/kg at 1.575 GHz and 0.160 W/kg at 2.45 GHz. Also, these results suggest that SAR values without the AMC plane, at both frequencies, are higher than the values observed for the antenna with the AMC plane. It can also be observed that the antenna when bent at both axes and assessed near the shoulder produced slightly lower values compared to the SAR values produced when placed in proximity of the upper arm. This can be due to the composition of the shoulder area which consists of more skin and bone in comparison to the upper arm which contain more absorptive muscle and fat tissues.

A summary of the on-body bandwidth, FBR and SAR at both frequencies is provided in Table III. The simulated and measured radiation patterns of the bent antennas at 1.575 GHz and 2.45 GHz when located on-body are shown in Figure 11(a-d). It can be observed that the antenna radiated towards the forward direction with low backlobes. A minor discrepancy can be observed between simulation and measurements Figure 11(b) due to measurement complexities, for example, while doing on-body measurements, the probe was found to be not entirely bent as compared simulations and has led to the measurement inaccuracies. However, the proposed antenna still maintained radiation in forwards direction with low back lobes. Also, measured cross-polarization levels are below -20 dB in each case.

A comparison of the proposed structure with state-of-art multiband antennas designed with dual, linear and circular polarization is provided in Table IV. Compared to previous researches, it is evident that the proposed antenna achieved improvement relative to recent multiband and dual-polarized planar antennas, especially in terms of fractional impedance and axial ratio bandwidths.

IV. CONCLUSION

A wearable textile antenna with dual-band and dual-sense characteristics is designed for location tracking purposes, using GPS in the outdoor and WLAN in indoor environments. The dual band radiator originated from a square patch before being integrated with slits and truncated corners to operate in the 1.575 GHz band (with circular polarization) and in the 2.45 GHz band (with linear polarization). To alleviate body coupling in wearable antennas, an AMC plane with a 3 × 3 array of unit cells is integrated behind the antenna. The AMC unit cells are designed based on a square patch with rectangular slits on each side, and a square ring for operation at 2.45 GHz.

The generated fractional impedance bandwidth in these two bands is 27 % and 7.5 %, respectively, with a 9 % 3 dB axial ratio bandwidth in the 1.575 GHz band. Meanwhile, its realized gain at 1.575 GHz is 1.98 dBic, and is 1.94 dBi at 2.45 GHz. Further investigation of the antenna under bending indicated its better suitability for operation when bent at the *y*-axis on body. The antenna integrated with the AMC plane provided SAR values which are below 0.12 W/kg for placement on the upper arm and shoulder of a human body. This is due to the front to back ratio which is always above 10 dB, and is below the regulatory limit of 2W/kg, thus making it suitable for wearable applications.

REFERENCES

[1] M. S. Shakhirul et al, "Textile Antenna with Simultaneous Frequency and Polarization Reconfiguration for WBAN", *IEEE Access*, vol. 6, pp. 7350-7358, 2018.

[2] N. F. M. Aun, P. J. Soh, A. A. Al-Hadi, M. F. Jamlos, G. A. E. Vandenbosch and D. Schreurs, "Revolutionizing Wearables for 5G: 5G Technologies: Recent Developments and Future Perspectives for Wearable Devices and Antennas," *IEEE Microwave Magazine*, vol. 18, no. 3, pp. 108-124, May 2017.

[3] Human Exposure to Radio Frequency Fields from Hand-held and Body-mounted Wireless Communication Devices – Human Models, Instrumentation and Procedures, *IEC 62209 Standard*, 2010.

[4] G. Z. Rafi, M. Mohajer, A.Malarky, P. Mousavi, and S. Safavi-Naeini, "Low-profile integrated microstrip antenna for GPS-DSRC application," *IEEE Antennas and Wireless Propagation Letters*, vol. 8, pp. 44–48, 2009.

[5] S. L. Ma and J. S. Row, "Design of Single-Feed Dual-Frequency Patch Antenna for GPS and WLAN Applications," *IEEE Transactions on Antennas and Propagation*, vol. 59, no. 9, pp. 3433-3436, Sept. 2011.

[6] P. Sharma and K. Gupta, "Analysis and optimized design of single feed circularly polarized microstrip antennas," in IEEE Transactions on Antennas and Propagation, vol. 31, no. 6, pp. 949-955, November 1983.

[7] Nasimuddin, X. Qing and Z. N. Chen, "Compact Asymmetric-Slit Microstrip Antennas for Circular Polarization," IEEE Transactions on Antennas and Propagation, vol. 59, no. 1, pp. 285-288, Jan. 2011.

[8] W.-S. Chen, C.-K. Wu and K.-L. Wong, "Novel compact circularly polarized square microstrip antenna," IEEE Transactions on Antennas and Propagation, vol. 49, no. 3, pp. 340-342, March 2001.

[9] R. P. Dwivedi, M. Z. Khan, and U. K. Kommuri, "UWB circular cross slot AMC design for radiation improvement of UWB antenna," *AEUE - International Journal of Electronics and Communications*, vol. 117, 2020.

[10] N. Hussain, M. Jeong, A. Abbas, T. Kim and N. Kim, "A Metasurface-Based Low-Profile Wideband Circularly Polarized Patch Antenna for 5G Millimeter-Wave Systems," in IEEE Access, vol. 8, pp. 22127-22135, 2020.

[11] N. Hussain, M. Jeong, J. Park and N. Kim, "A Broadband Circularly Polarized Fabry-Perot Resonant Antenna Using A Single-Layered PRS for 5G MIMO Applications," IEEE Access, vol. 7, pp. 42897-42907, 2019.

[12] W. Cao, B. Zhang, A. Liu, T. Yu, D. Guo, and Y. Wei, "Gain Enhancement for Broadband Periodic Endfire Antenna by using Split-Ring Resonator Structures," *IEEE Transactions on Antennas and Propagation*, vol. 60, no.7, pp. 3513- 3516, Jul. 2012.

[13] T. Yue, Z. H. Jiang and D. H. Werner, "A Compact Metasurface-Enabled Dual-Band Dual-Circularly-Polarized Antenna Loaded With Complementary Split Ring Resonators," *IEEE Transactions on Antennas and Propagation*, vol.67, no.2, pp. 794-803, Feb. 2019. (doi: 10.1109/TAP.2018.2882616)

[14] K. Agarwal, Nasimuddin and A. Alphones, "Wideband Circularly Polarized AMC Reflector Backed Aperture Antenna," in *IEEE Transactions on Antennas and Propagation*, vol. 61, no. 3, pp. 1456-1461, March 2013.

[15] J. Chen, K. Tong, A. Al-Armaghany and J. Wang, "A Dual-Band Dual-Polarization Slot Patch Antenna for GPS and Wi-Fi Applications," in *IEEE Antennas and Wireless Propagation Letters*, vol. 15, pp. 406-409, 2016. doi: 10.1109/LAWP.2015.2448536

[16] M. E. de Cos, F. L. Heras and M. Franco, "Design of Planar Artificial Magnetic Conductor Ground Plane Using Frequency-Selective Surfaces for Frequencies Below 1 GHz," in IEEE Antennas and Wireless Propagation Letters, vol. 8, pp. 951-954, 2009. doi: 10.1109/LAWP.2009.2029133

[17] Dewan R, Rahim MK, Hamid MR, Yusoff MF, Samsuri NA, Murad NA, Kamardin K. Artificial magnetic conductor for various antenna applications: An overview. International Journal of RF and Microwave Computer-Aided Engineering. 2017 Aug;27(6):e21105.

[18] E. F. N. M. Hussin *et al*., "Dual-band dual-polarized textile antenna for location tracking in AAL," *12th European Conference on Antennas and Propagation (EuCAP 2018)*, London, 2018, pp. 1-4.

[19] S. Maci and G. B. Gentili, "Dual-frequency patch antennas," *IEEE Antennas and Propagation Magazine*, vol. 39, no. 6, pp. 13-20, Dec. 1997.

[20] C. Balanis, *Antenna theory : analysis and design*, 3rd ed. Wiley, 2005.

[21] R.Garg, P. Bhartia, I.J. Bahl and A. Ittipiboon, *Microstrip antenna design handbook*, Artech house, 2001.

[22] D. Pozar and B. Kaufman, "Comparison of three methods for the measurement of printed antenna efficiency," *IEEE Transactions on Antennas and Propagation*, vol. 36, no. 1, pp. 136–139, 1988

[23] P. Salonen, and Y. Rahmat-Samii, "Textile antennas: Effects of antenna bending on input matching and impedance bandwidth." In *IEEE First European Conference on Antennas and Propagation*, (EuCAP), Nice, France, 2006, pp. 1-5.

[24] G. Goussetis, A. P. Feresidis and J. C. Vardaxoglou, "Tailoring the AMC and EBG characteristics of periodic metallic arrays printed on grounded dielectric substrate," in *IEEE Transactions on Antennas and Propagation*, vol. 54, no. 1, pp. 82-89, Jan. 2006. doi: 10.1109/TAP.2005.861575

[25] Ito K, Lin CH, Lin HY, Chen ZN, Liu D, Nakano H, Qing X, Zwick T. *Evaluation of wearable and implantable antennas with human phantoms*. Handbook of antenna technologies. Springer, Singapore. 2015:1-24.

[26] S. Liu, S. Qi, W. Wu and D. Fang, "Single-fed dual-band dual-polarized U-slot patch antenna," in *2013 IEEE MTT-S International Microwave Workshop Series on RF and Wireless Technologies for Biomedical and Healthcare Applications (IMWS-BIO)*, Singapore, 2013, pp. 1-3.

[27] M. Rahimi, A. Keshtkar, F. B. Zarrabi and R. Ahmadian, "Design of Compact Patch Antenna Based on Zeroth-Order Resonator for Wireless and GSM Applications with Dual Polarization," *AEU-International Journal of Electronics and Communications*, vol. 69, no. 1, pp. 163-168, Jan. 2015.

[28] X. F. Chen and Y. J. Zhao , "Dual-band polarization and frequency reconfigurable antenna using double layer metasurface," *AEU - International Journal of Electronics and Communications*, vol. 95, pp. 82-87, Oct. 2018.

[29] J. Lin, Z. Qian, W. Cao, S. Shi, Q. Wang and W. Zhong, "A Low-Profile Dual-Band Dual-Mode and Dual-Polarized Antenna Based on AMC," *IEEE Antennas and Wireless Propagation Letters*, vol. 16, pp. 2473-2476, 2017.

[30] K. N. Paracha et al, "A Low-Profile, Dual-Band and Dual-Polarized Antenna for Indoor/Outdoor Wearable Application", *IEEE Access*, vol 7, pp. 33277-33288, 2019.